buildings

MDPI

Article

Influences of Species and Density on the Horizontal Flame Spread Behavior of Densified Wood

Yang Zhou [1], Wenxi Qiu [1], Penghui Zhou [1], Zhengyang Wang [1,*], Xiaonan Zhang [2], Xiangyu Mao [3] and Rongwei Bu [1]

[1] Department of Fire Protection Engineering, Central South University, Changsha 410075, China
[2] Hunan Vocational Institute of Safety Technology, Changsha 410075, China
[3] Department of Electrical and Computer Engineering, Georgia Institute of Technology, Atlanta, GA 30332, USA
* Correspondence: zywang102@csu.edu.cn

Abstract: Densified wood possesses outstanding mechanical properties and serves as a desired construction material for modern timber buildings. However, the limited research on its flame behavior hinders its broader applications. The authors of this paper experimentally and analytically investigated the influence of wood species and density on horizontal flame spread behavior. Densified oak and densified fir were tested. The flame spread rate decreased with wood density in both densified wood types. Their values were close at the same density. The mass loss rate ($\dot{m}$) of the densified wood decreased with the increase in wood density. The densified oak had higher $\dot{m}$ due to its lower lignin content. Dimensionless correlations between the $\dot{m}$ and density were obtained which agree with the experiments. The flame heights (L_f) of the densified wood also decreased with the increase in wood density. The densified oak had higher L_f due to its higher $\dot{m}$. As the densified wood density increased, the radiation (and conduction) was reduced (and enhanced), but the convection remained constant. The densified oak had lower convection, lower conduction, and higher radiation than the densified fir at the same density. Gas-phase heat transfer was dominant in the flame spread of the densified wood, but conduction was also significant as its contribution can be as high as 70% of gaseous heat transfer.

Keywords: densified wood; density; flame spread; wood species

Citation: Zhou, Y.; Qiu, W.; Zhou, P.; Wang, Z.; Zhang, X.; Mao, X.; Bu, R. Influences of Species and Density on the Horizontal Flame Spread Behavior of Densified Wood. *Buildings* **2024**, *14*, 620. https://doi.org/10.3390/buildings14030620

Academic Editor: Karim Ghazi Wakili

Received: 20 January 2024
Revised: 18 February 2024
Accepted: 22 February 2024
Published: 27 February 2024

1. Introduction

The merits of green building, which is an important method for the construction industry in achieving carbon neutrality, include energy saving, environmental protection, and negative carbon emissions [1,2]. However, the current construction industry relies heavily on concrete and steel. These two building materials have large energy costs and carbon emissions during their processes of production and utilization. Renowned for its plentiful resources and eco-friendliness, wood plays a significant role in the construction realm and has become an important green building material alternative [3,4]. Previous research reported that its substitution for concrete and steel could reduce carbon emissions in the construction industry by 31% [5]. Densified wood has excellent mechanical performance, higher than many traditional construction materials, presenting promising potential in applications in medium- and high-rise timber buildings [6,7]. Nevertheless, the fire safety of densified wood is hardly known, and due to the flammable nature of wood [8,9], it deserves to be investigated to improve its application. The results would be significant for evaluating the fire behavior of wooden structures constructed with dense wood.

The flame spread on a fuel surface is an important phenomenon in the transition of building fires from the initial stage to the fast-developing stage. The main influential factors on the flame spread over solid fuel include the specimen characteristics (density [10,11], moisture content [12], thickness [13], and width [14], etc.), spatial distributions (orientation [15] and fuel continuity [16], etc.), and external ambience (radiation [17], oxygen

concentration [18], etc.). Compared to natural wood, densified wood presents distinct characteristics, including varied weight fractions of cellulose, hemicellulose, and lignin, and controllable structural densities. [19]. Component fractions determine the microscale pyrolysis but have a weak effect on the combustion behavior and flame spread [20,21]. Therefore, structural density is an important factor influencing the flame spread behavior of densified wood.

This influence has been investigated previously. Di Blasi [22] discovered that increasing the thermal conductivity along the parallel direction of the flame spread had no impact on the flame spread velocity, but enhancing the thermal conductivity along the vertical flame spread direction increased the thermal penetration depth and decreased the flame spread rate. Similar conclusions were subsequently drawn by Kobayashi [23] based on flame spread tests of carbon-fiber-reinforced polymers. However, these conclusions were obtained from either theoretical calculations or non-charring polymer tests, which might not be valid for charring wood. Previous work [10] investigated the flame spread rate of various woods and observed a decrease in the flame spread rate as the density increased. A similar trend was noted by Quintiere [24], where the flame spread rate decreased with an increase in wood density under radiant heat flux conditions. The above conclusion pertains to a change in density achieved by altering the wood species. However, the limited impact of the components on flame spread cannot be precisely quantified or eliminated. The flame spread behavior of densified wood was recently investigated [11]. It was found that the flame spread rate, mass loss rate, and flame height all decreased with an increase in density. In addition, the increased density decreased the flame radiation, causing a shift in the gas-phase heat transfer from radiative-dominated to convection-dominant. However, only one wood species was used for the experiments, and the conclusions were not validated in different wood species.

The combustion behavior of wood varies with species. In general, wood is categorized as hardwood or softwood, with major distinctions in the weight fractions of three major components [25]. Hao et al. [26] compared the combustion behaviors of oak, larch, and red cedar. Red cedar (a typical softwood) exhibited a short ignition time, the lowest heat release, a slower flame spread rate, the fastest charring rate, and higher fire resistance, which was attributed to its relatively high lignin content. Wang et al. [12] investigated the flame spread behaviors of discretely distributed beech, fir, pine, camphor, and elm. The results showed that the total burning duration of samples with high moisture and density was considerably higher. Softwood, with higher lignin content and lower hemicellulose content, has a faster flame spread rate. Chen et al. [27] studied the flame spread behaviors of six decorative wood boards at various temperatures and wind speeds. These woods showed obvious distinctions in their rates and durations of flame spreads. However, the fundamental reason and the heat transfer mechanism were not clearly revealed. Different wood species have varied moisture content, composition content, and structure. These factors all have a significant influence on the flame spread behavior. Therefore, simply comparing the flame spread behaviors of natural wood among different species cannot achieved the same results as a single-factor variable test to reveal the influence of these factors on the flame spread of wood. By using the densified wood preparation method, it is possible to obtain different densities of the same wood (same component fraction). In this way, the effect of wood density on flame spread behavior can be studied. In addition, it is also possible to prepare woods of different species (different component fractions) with the same density. Then, the importance of wood components in flame spread behavior can be understood.

To summarize, the existing research has not fully revealed the influence of density on wood flame spread. Although a recent paper addressed this issue by investigating the flame spread behavior of densified wood, only one wood species was used [11]. This study is the first to explore the effect of density on flame spread behaviors in different wood species. Typical hardwood (oak) and softwood (fir) were chosen. The study aims to elucidate the impact of density on flame spread behavior, examine the variation in this

impact among different wood species, and explore the importance of wood components on flame spread behavior. The results will provide a deeper fundamental insight into the flame spread theory of wood materials. It also enhances the fire prevention capabilities of wood (densified wood) structure buildings, contributing significantly to the further development of green buildings in the construction industry.

2. Experiments

2.1. Experimental Materials

In this research, typical hardwood (oak) and softwood (fir) were selected and acquired from Fulin Group Co., Ltd., Changsha, China. Wood plates were cut into dimensions of 300 mm in length, 50 mm in width, and various thicknesses of 2 mm, 2.5 mm, 3 mm, 3.5 mm, and 4 mm. Sodium hydroxide (NaOH, >97%) and sodium sulfite (Na_2SO_3, >98%) were procured from Shanghai Hongjie Chemicals Co., Ltd., Shanghai, China, and deionized water was supplied by Zhejiang Nandai Industrial Co., Ltd., Wenzhou, China.

2.2. Preparation of Densified Wood

The preparation of densified wood was consistent with previously published work [28,29]. Natural woods were delignified in 1 L of a mixed solution consisting of 2.5 mol/L NaOH and 0.4 mol/L Na_2SO_3 for 6 h. The treated samples were washed with deionized water and dried in an oven at 60 °C for 24 h to obtain lignified wood. The delignified wood was hot-pressed by a plate vulcanizer. The pressure and time of the hot-press were varied according to the initial thickness of the wood to receive a constant final compressed thickness of 2 mm. The compressed wood was dried in an oven at 60 °C for 12 h to obtain densified wood. After densification treatment, the porosity of the cells decreased, and the density and structural characteristics of the wood changed. The densities of natural wood (ρ_0) were 446.67 kg/m^3 for fir and 731.20 kg/m^3 for oak. After densification treatment, the densities (ρ) of densified fir ranged from 463.33 kg/m^3 to 906.67 kg/m^3, and those of densified oak ranged from 830.83 kg/m^3 to 1343.05 kg/m^3. Thus, the density ranges of densified fir and densified oak overlapped from 731.20 kg/m^3 to 906.67 kg/m^3. Before the density measurement and flame spread experiment, samples were oven-dried to fully mitigate the influence of moisture content.

2.3. Experimental Apparatus

Figure 1 illustrates the flame spread experimental system schematic. The experimental system comprises a rotating bracket system and a data acquisition system. The rotating bracket system includes an experimental bracket, thermal insulation board, and tested samples. The data acquisition system was employed to measure the flame spread characteristics of the sample during the experiment. It consisted of a high-precision electronic balance (Sartorius PMA35001, precision 0.1 g, frequency 5 Hz, range 0–35 kg, Sartorius, Gottingen, Germany), two high-definition cameras (SONY FDR-AX-100E and SONY FDR-AX-700, Sony, Tokyo, Japan), a K-type thermocouple (WRNK-191, Shanghai Automation Instrumentation Co., Ltd., Shanghai, China), a data acquisition device, and a personal computer.

The sample was positioned horizontally on a rotatable holder. Two cameras were positioned on the front and one side of the sample to record the evolution of flame spread. K-type thermocouples were used to measure the solid-phase temperature on the back side of the wood. These thermocouples were wrapped in tin foil to mitigate uncertainty from flame heating. A flame recognition algorithm was used to determine the flame form (flame front position and flame height). Based on the threshold method from previous works [30,31], critical greyscale values were obtained. The greyscale values of the pixels with lower (or higher) than this critical value changed to 0 (or 1). This led to a black-and-white image indicating the flame shape. Once the pixel baselines of the flame spread threshold position and the wood surface were defined, the largest pixel distance from the flame to the flame spread threshold position (and the wood surface) was obtained as the flame front pixel position (and the flame pixel length). If the pixel-to-length ratio of

the images is pre-calibrated before the experiments, the pixel length (or position) can be converted to the real length (or position). In the end, the evolution of flame heights and flame front positions were obtained along with the experimental time. The instantaneous flame spread rate was determined by calculating the increasing rate of the flame front position. The data were obtained by averaging the values in the steady stage, while the upper and lower bars of the data refer to the minimum to maximum values.

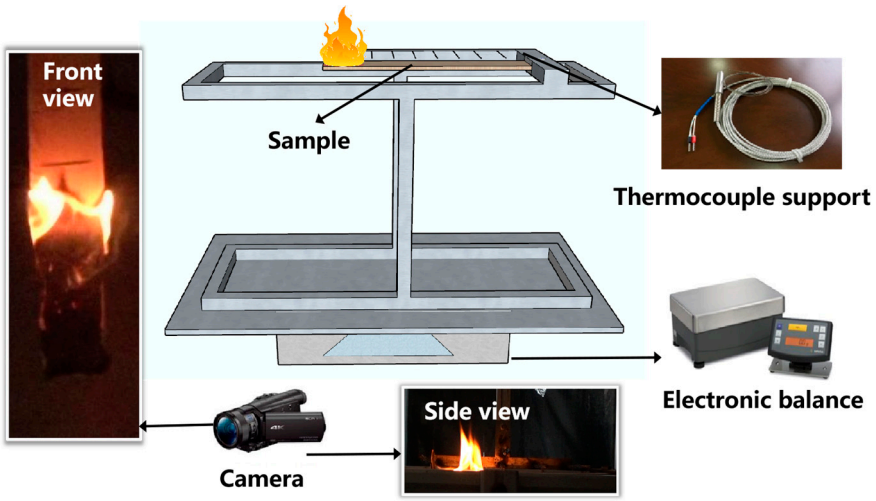

Figure 1. Flame spread experimental system schematic.

3. Results and Discussion

3.1. Typical Flame Form

Figure 2 displays typical images of surface flame spread behavior for densified fir (ρ = 896.67 kg/m^3). Due to the flame flickering, the flame height fluctuated throughout the entire flame spread process. It is evident from Figure 2 that the flame spread of densified fir and densified oak comprised three stages: the unsteady stage, steady stage, and burnout stage. As depicted in Figure 2a, the flame height gradually increased during the flame unsteady stage. Upon entering the steady stage, the flame height stabilized. The front view in Figure 2b illustrated that, with time, the flame consistently spread along the surface of the wood towards the forward unburned area. In the steady stage, the pyrolysis front appeared as an approximately straight line, but the flame shape at the lateral sides were noticeably larger than that in the middle of the plate. Due to air entrainment, the airflows at lateral sides were more intense, leading to increased gas release from pyrolysis and a larger flame shape. Ultimately, as the flame burned to the end of the plate, the flame height gradually decreased due to insufficient fuel. In the case of densified oak, its flame height exhibited a stronger flickering in the unsteady stage. It had a faster extinguishing speed and a shorter combustion duration. The flame spread behaviors in the steady stage were primarily analyzed and used to capture the flame spread characteristics of samples.

3.2. Flame Spread Rate

Flame spread rate is a critical factor in evaluating fire risk. The flame spread rate for each test was averaged over the instantaneous flame spread rate of the steady stage. Figure 3 illustrates the correlation between flame spread rate and the density of different wood. As density increased, the flame spread rate decreased for densified fir; in comparison, the flame spread rate for densified oak had a larger uncertainty, but it also decreased with the increase in density. At the same density range (ρ = 731.20–906.67 kg/m^3), the flame spread rate of densified oak was slightly higher than that of densified fir, but the difference in flame spread rate was less than the uncertainty. This suggests that the influence of wood species on flame spread rate was negligible compared to that of wood density.

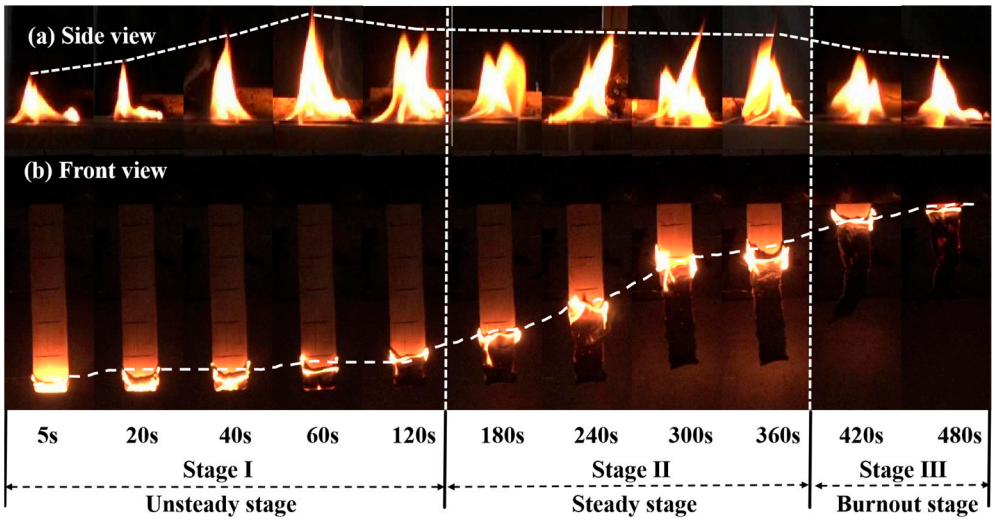

Figure 2. (**a**) Front view and (**b**) side view image sequences of a typical densified fir flame spread (ρ = 896.67 kg/m^3).

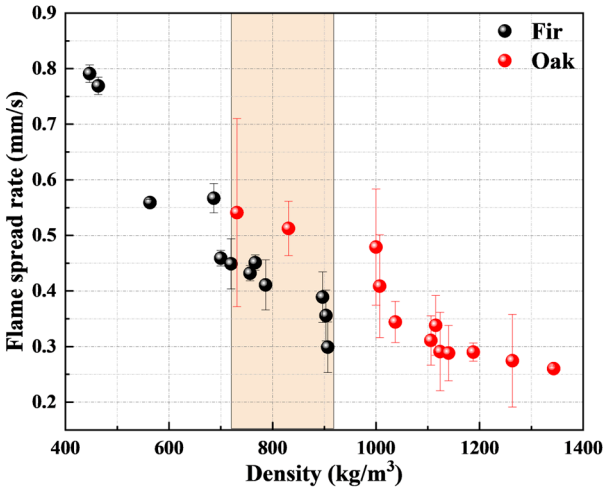

Figure 3. Experimental flame spread rates of densified oak and densified fir with different densities. The colored area indicates the overlapped density for both densified wood types.

3.3. Mass Loss Rate

Figure 4 illustrates the variation in mass loss rate ($\dot{m}$) with density in densified fir and densified oak. Similar to the flame spread rate (Figure 3), $\dot{m}$ of both densified fir and densified oak decreased with the increase in density. This was attributed to the wood with higher density having a higher thermal inertia. The wood temperature increase was attenuated, leading to a reduction in the pyrolysis gas release rate. Thus, $\dot{m}$ was decreased and was in the ranges of 15–40 mg/s for densified fir and 20–70 mg/s for densified oak. The maximum $\dot{m}$ of densified oak was 1.75 times higher than that of densified fir. Its $\dot{m}$ was reduced at a faster rate along with the increase in density. When densified oak and densified fir had the same density (between 731.20 and 906.67 kg/m^3), $\dot{m}$ of densified oak was significantly higher than that of densified fir. This can be attributed to the densified fir having a higher lignin content and a higher char yield during the combustion [28].

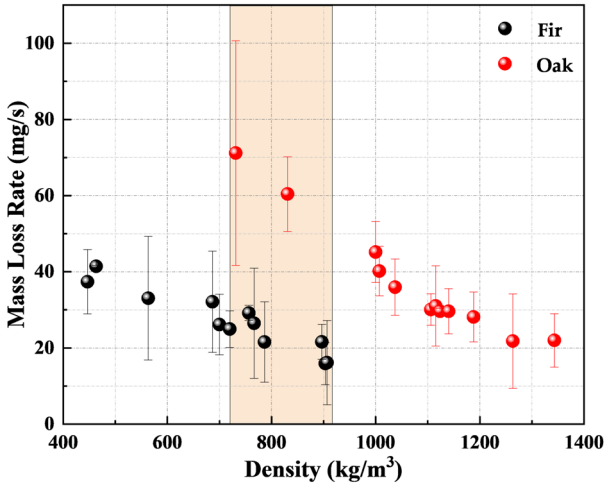

Figure 4. The measured mass loss rate of densified fir and densified oak with different densities. The colored area indicates the overlapped density for both densified wood types.

To better evaluate the impact of wood density on the mass loss rate, based on previous work [11], the relationship between the dimensionless mass loss rate ($m/\rho_0 W d v_{f,\rho 0}$) and dimensionless density (ρ/ρ_0) is shown in Figure 5.

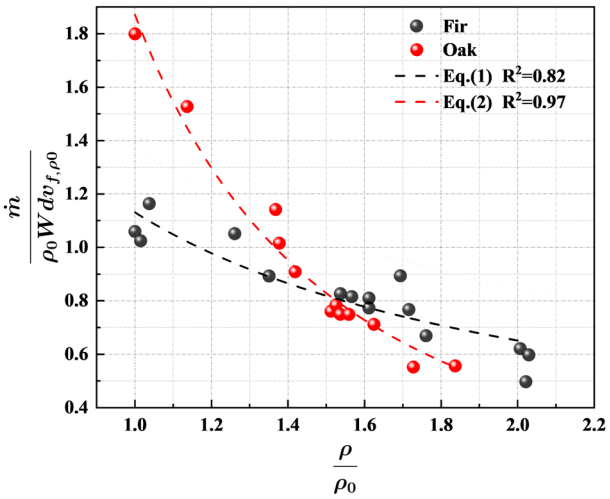

Figure 5. Correlation between dimensionless mass loss rates and dimensionless wood densities between densified oak and densified fir.

Similar to the evolution trend in Figure 4, $m/\rho_0 W d v_{f,\rho 0}$ decreased with the increase in ρ/ρ_0. These experimental trends were fitted to the Equations (1) and (2) for densified fir and densified oak, respectively.

$$\dot{m}/\rho_0 W d v_{f,\rho 0} = 1.13(\rho/\rho_0)^{-0.80} \quad (1)$$

$$\dot{m}/\rho_0 W d v_{f,\rho 0} = 1.87(\rho/\rho_0)^{-2.01} \quad (2)$$

where W is the wood width, d is the material thickness, $v_{f,\rho 0}$ is the flame spread rate of natural wood. The predicted curves were compared with the test results with R^2 of 0.82 for densified fir and 0.97 for densified oak, indicating a good fit.

3.4. Flame Height

Flame height (L_f) is relative to the heat release rate of the wood combustion and thus is an important flame spread characteristic. L_f is defined as the vertical distance between

the flame top and the wood surface (white line in Figure 2). For each test, L_f was calculated by averaging the instantaneous L_f during the steady stage. Figure 6 illustrates the variation in L_f with density for both densified fir and densified oak. The evolution of L_f was similar to that of $\dot{m}$. It decreased with the wood density of both densified wood types, while the densified oak had higher L_f than the densified fir. The decreased L_f along with the increased density for both densified wood types could be attributed to two factors. First, the increase in density resulted in higher thermal inertia. This reduced the increase rate of wood temperature and thus reduced the rate of pyrolysis gas production. Second, a layer of densified char was formed in densified wood. This condensed char layer hardly cracked, which decelerated the release rate of pyrolysis gases [4,28,29]. The combination of these two factors leads to a decrease in L_f as the wood density increased. The L_f of densified fir ranged from 25 mm to 60 mm, while that of densified oak ranged from 40 mm to 70 mm. The broader range of flame height variation in densified fir compared to densified oak indicated a stronger influence of density, resulting in a faster descent rate. When compared the densified oak and densified fir with similar densities (ρ = 731.20–906.67 kg/m^3), the densified oak presented a higher L_f. This could be due to its higher $\dot{m}$. More pyrolysis gases were released from the wood and facilitated the flaming combustion. This indicated that wood species had an important impact on $\dot{m}$ and L_f of flame spread.

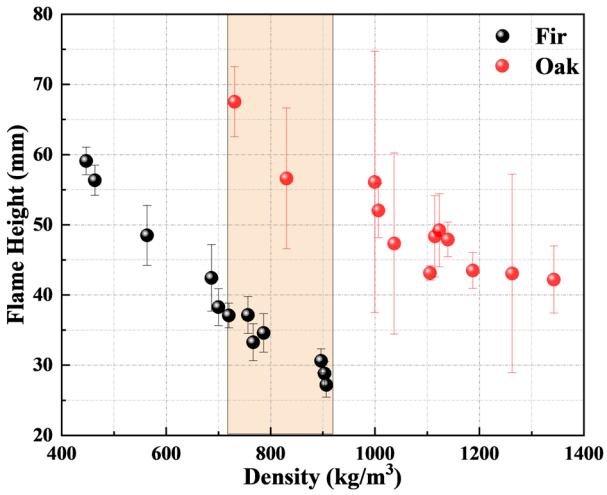

Figure 6. Measured flame heights at different densified oak and densified fir densities. The colored area indicates the overlapped density for both densified wood types.

Previous studies indicated an exponential correlation between dimensionless flame height (L_f^*) and dimensionless heat release rate (Q^*) [32–34]. L_f^* and Q^* are defined as

$$L_f^* = L_f / W \tag{3}$$

$$Q^* = \frac{\dot{Q}}{\rho_\infty C_{p,\infty} T_\infty \sqrt{g} W^{5/2}} \tag{4}$$

where ρ_∞ and $C_{p,\infty}$ are the air density and air specific heat, respectively, and T_∞ and g are the ambient temperature and the acceleration of gravity, respectively, which can be found in Appendix A. $\dot{Q}$ represents the heat release rate, which was calculated as follows [11].

$$\dot{Q} = \dot{m} \Delta H_c \tag{5}$$

where ΔH_c is the heat of combustion of pyrolyzed gases. Figure 7 illustrates the relationship between L_f^* and Q^* of densified fir and densified oak. Despite notable differences in mass loss rate (Figure 4) and flame height (Figure 6) between densified fir and densified oak at the equivalent density, the relationship between L_f^* and Q^* remained consistent. This is

because a higher mass loss rate results in more gases contributing to the flaming combustion (higher flame height). In addition, the relationship between L_f^* and Q^* largely depended on the combustion characteristics (e.g., ΔH_c) of pyrolysis gases. Although densified fir and densified oak were different in wood species, their major components and corresponding weight fractions were all lignin, cellulose, and hemicellulose. As a result, the types and the amounts of their pyrolysis gases were also similar. Therefore, their relationships between L_f^* and Q^* could be regarded as similar and were fitted as a curve.

$$L_f^* = 0.62Q^{*0.52} \tag{6}$$

The predictions of Equation (6) correlate to the experimental measurements with an R^2 of 0.75. All results were within 25% of the uncertainty.

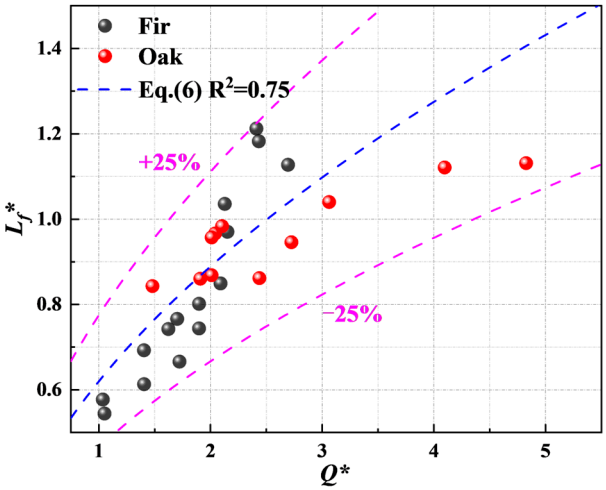

Figure 7. Power-law correlations between L_f^* and Q^* of densified oak and densified fir.

3.5. Heat Transfer Behavior

The samples in this work were constantly 2 mm in thickness and could be characterized as thermally thin material [11,12]. For the horizontal flame spread of thermally thin wood, the preheating zone was mainly subjected to the solid-phase heat conduction from the pyrolysis zone and the radiative and convective heat transfers of the gaseous flame (Figure 8).

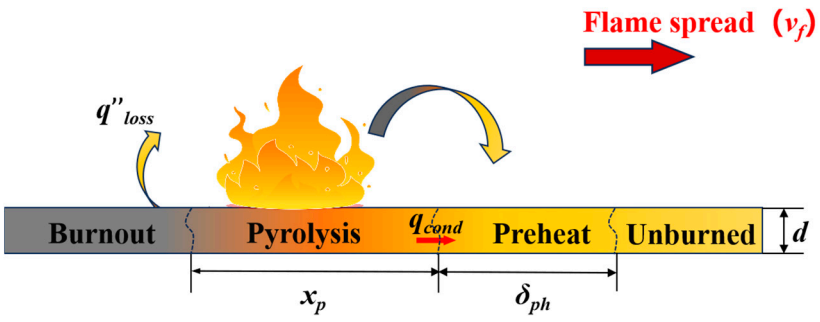

Figure 8. Heat transfer schematic for horizontal flame spread of densified wood.

The heat conduction $(\dot{q}''_{cond})$ can be represented by the Fourier equation.

$$\dot{q}''_{cond} = k_x(\partial T/\partial x)_{T_{char}} = [k_x(\partial T/\partial t)_{T_{char}}]/v_f \tag{7}$$

where k_x is the thermal conductivity of densified wood along the flame spread, and $\partial T/\partial x$ is the temperature gradient of the wood per unit length. It can be obtained by dividing the

$\partial T\, v_f/\partial t$ (temperature gradient of the wood per unit time) to the flame spread rate. T_{char} was the characteristic temperature ($T_{char} = (T_P + T_s)/2$), which was the average of pyrolysis temperature (T_P) and initial wood surface temperature (T_s). Previous work found that the thermal conductivities of wood in different species (softwood and hardwood) varied according to their moisture content, temperature, and density [35]. Therefore, according to the thermal conductivity measurements of densified wood [11], the thermal conductivity of both densified fir and densified oak in the longitudinal direction can be calculated as

$$k_x = [(0.13403 + 0.004064M)(\rho/1000) + 0.10403](T_s/297) \quad (8)$$

where M represents the moisture content of the wood, which was measured according to ISO 13061-1 [36], and the moisture was measured to be 12.7% and 10.4% for densified fir and densified oak, respectively. The evolution of wood temperatures was measured by thermocouples. A typical result of densified oak with a density of 731.20 kg/m^3 is shown in Figure 9.

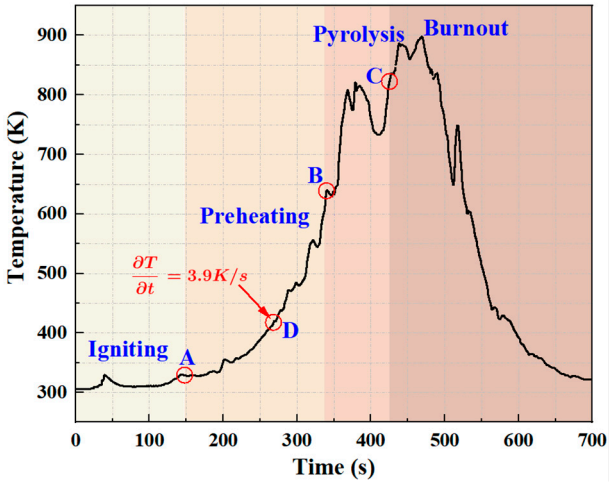

Figure 9. Typical temperature evolution of wood in steady stage (densified oak, ρ = 731.20 kg/m^3).

The evolution of wood temperature could be classified into three stages: the preheating stage (AB), the pyrolysis stage (BC), and the burnout stage (after point C). A refers to the time that wood was heated; B refers to the time to reach the pyrolysis temperature (600 K) [37], from which points A to B were determined to be the preheating stage; and C refers to the time to reach char oxidation temperature (844 K), which is the critical temperature of char oxidation [28]; thus, points B to C were the pyrolysis stage, and after point C was the burnout stage. The densified fir had a similar char oxidation temperature but a lower pyrolysis temperature (588 K [28]) than densified oak. In Equation (7), the slope of point D (characteristic temperature) in Figure 9 was taken as $(\partial T/\partial t)_{char}$ for calculation.

The heat conduction of wood samples was calculated by using Equation (7). Results are shown in Figure 10. Heat conductions of both densified oak and densified fir increased with wood density because of their enhanced thermal conductivities. When comparing the densified oak and densified fir with similar densities (ρ = 731.20–906.67 kg/m^3), densified fir had higher heat conduction than densified oak because the flame spread rate of densified fir was slightly lower than that of densified oak (Figure 3).

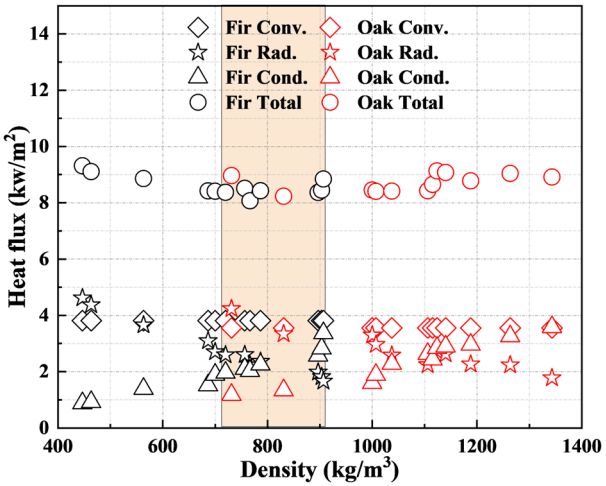

Figure 10. Calculated radiative heat, convective heat, conductive heat, and total heat fluxes with different densified fir and densified oak densities. The colored area indicates the overlapped density for both densified wood types.

To further study the main heat transfer characteristics of flame spread, the radiant heat, convective heat, and total heat flow were calculated. The expression for the convective heat ($\dot{q}''_{f,c}$) is [38,39]

$$\dot{q}''_{f,c} = h\left(T_f - T_p\right) \tag{9}$$

where h and T_f are the convective heat transfer coefficient and flame temperature, respectively. h is related to the Nusselt number ($\overline{Nu}$) represented as [40]

$$\overline{Nu} = \frac{hl}{k_g} \tag{10}$$

where l represents the characteristic length, which approximates to the wood width; k_g represents the thermal conductivity of air (Appendix A). The horizontal flame spread can be regarded as [41]

$$\overline{Nu}_{L,\theta=0} = 0.27Ra_L^{1/4}, 10^5 \le Ra_L \le 10^{10} \tag{11}$$

The Rayleigh number (Ra_L) is

$$Ra_L = \frac{g\beta\left(T_f - T_p\right)l^3}{\nu\alpha} \tag{12}$$

where β, v, and α are the coefficient of thermal expansion, the kinematic viscosity coefficient, and the thermal diffusivity, respectively. Their values are also listed in Appendix A. Combining Equations (9)–(12), the convection heat can be calculated as Equation (13) and is shown in Figure 10.

$$\dot{q}''_{f,c} = \frac{0.27k_g}{l}\left(\frac{g\beta\left(T_f - T_p\right)l^3}{\nu\alpha}\right)^{0.25}\left(T_f - T_p\right) \tag{13}$$

Heat convection did not vary with the density, so both densified oak and densified fir had constant heat convection in this work. The difference in their heat convection was mainly due to their different material properties (e.g., T_P). The densified oak had higher T_P than densified fir, so its convective heat was smaller.

The radiative heat ($\dot{q}''_{f,r}$) can be represented by the Stefan–Boltzmann equation [42].

$$\dot{q}''_{f,r} = \varepsilon\sigma F\left(T_f^4 - T_s^4\right) \tag{14}$$

where σ and ε are the Boltzmann constant and the flame emissivity, respectively, which can be found in Appendix A. ε is affected by the flame height [43].

$$\varepsilon = 1 - \exp\left(k_s L_f\right) \tag{15}$$

where k_s represents the absorption coefficient of the flame. Its value varies from 0.1 to 1 m^{-1}. In this work, the value was taken as 1 m^{-1}. F is the view factor, expressed as [44]

$$F = \frac{1}{\pi}\left[\arctan\left(\frac{W}{2\delta_{ph}}\right) + \left(\frac{L_f - \delta_{ph} + L_f\cos\theta}{\sqrt{\delta_{ph}^2 + L_f^2 - 2L_f\delta_{ph}\cos\theta}}\right)\arctan\left(\frac{W}{2\sqrt{\delta_{ph}^2 + L_f^2 - 2L_f\delta_{ph}\cos\theta}}\right) + \frac{W\sin\theta + W\cos\theta}{2\sqrt{\delta_{ph}^2\sin^2\theta + W^2/4}}\left(\arctan\left(\frac{\delta_{ph}\cos\theta}{\sqrt{\delta_{ph}^2\sin^2\theta + W^2/4}}\right) + \arctan\left(\frac{L_f - \delta_{ph}\cos\theta}{\sqrt{\delta_{ph}^2\sin^2\theta + W^2/4}}\right)\right)\right] \tag{16}$$

where θ is the flame tilt angle. For this work, the flame was approximately perpendicular to the wood surface, so $\theta = 90°$. δ_{phh} is the preheating zone length, which is calculated as

$$\delta_{ph} = v_f t_{ph} \tag{17}$$

where t_{ph} is the preheating time, which can be measured by the wood temperature measurement shown in Figure 9. According to previous studies [11], δ_{ph} did not vary significantly with the increase in wood density, so an average of 25.09 mm for densified oak and 23.05 mm for densified fir were determined.

Radiative heat for both densified oak and densified fir calculated by Equation (14) are shown in Figure 10. They both showed decreasing tendencies with the increase in sample density. This was because L_f was decreased with the increase in density. This led to the decreased flame emissivity and view factor, resulting in decreased radiant heat flux. Consequently, as density increased, the dominant gas-phase heat transfer mode shifted from radiative-dominant to convection-dominant (Figure 10). The differences in heat radiation between densified oak and densified fir primarily arose from their different flame heights and preheating zone lengths. When comparing the densified oak and densified fir with similar densities (ρ = 731.20–906.67 kg/m^3), densified oak had a close view factor but a larger flame height than densified fir, resulting in higher flame emissivity. Thus, its heat radiation was higher.

For densified fir, the radiation decrease exceeded its conduction increase, leading to a slight reduction in total heat transfer (the summation of radiation, convection, and conduction) with the increase in density (Figure 10). Consequently, the flame spread rate was decreased with the increase in wood density (Figure 3). In comparison, the total heat transfer of densified oak exhibited an enhanced trend with density. Nevertheless, the flame spread rate of densified oak still decreased with the increase in wood density (Figure 3). Figure 11 shows the comparison between the solid-phase and gas-phase heat transfers. The ratio was enhanced with the increase in wood density. All values were less than 0.7, indicating that gas-phase heat transfer was dominant in the flame spread of densified wood. Nevertheless, the heat conduction accounted for at least 9.5% of total heat transfer. Its proportion rose with the increase in density, reaching a maximum of 70%. Its significance in the heat transfer analysis of flame spread cannot be overlooked. When comparing the densified oak and densified fir with similar densities (ρ = 731.20–906.67 kg/m^3), the proportion of solid-phase heat transfer in densified fir exceeded that in densified oak. This was because densified fir had higher conduction and lower radiation.

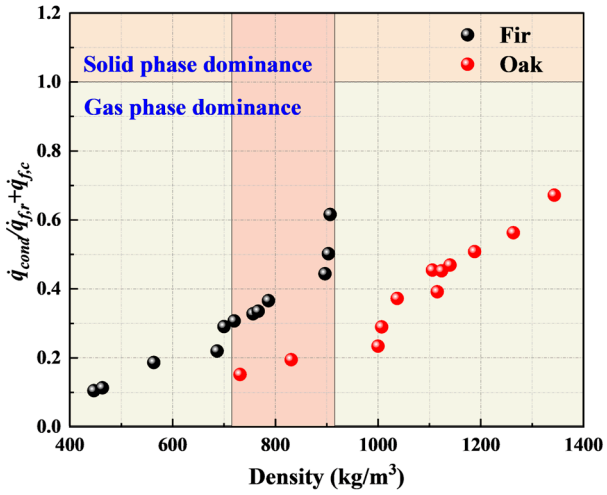

Figure 11. Comparison between the solid-phase and gas-phase heat transfers with different densified fir and oak densities.

4. Conclusions

This research investigated the horizontal flame spread behavior of densified wood across a broad density range. Typical softwood (fir) and hardwood (oak) were tested. Combined with theoretical analysis, the influence of sample density on the flame spread features and heat transfer mechanism were studied. Here are the major conclusions.

1. The flame spread rate was decreased with the increase in wood density. This trend was similar in both densified wood types. Their values were also close at the same density. This indicated that the influence of wood species on flame spread rate was negligible compared to that of wood density.
2. The mass loss rate of both densified wood types decreased with the increase in wood density due to the enhanced thermal inertia. The densified oak showed a higher mass loss rate than densified fir at the same density due to its lower lignin content (char yield). Correlations between dimensionless mass loss rate and dimensionless density were obtained, which agree with the experiments with an R^2 of 0.82 for densified fir and 0.97 for densified oak.
3. The flame height of both densified wood types decreased with the increase in wood density. The enhanced density reduced pyrolysis gas production. It formed a condensed char that also reduced the pyrolysis gases release. The densified oak showed a higher flame height than densified fir at the same density since it had a higher mass loss rate. The trend between the L_f^* and Q^* was similar for both densified wood types because their pyrolysis gases were similar.
4. As the wood density increased, radiation (and conduction) of densified wood was reduced (and enhanced), while convection remained constant. The densified oak had lower convection than densified fir due to its higher pyrolysis temperature. The densified oak showed lower conduction and higher radiation than densified fir at the same density. Overall, gas-phase heat transfer was dominant in the flame spread of densified wood, but conduction was significant in heat transfer analysis as its contribution could be as high as 70% of gaseous heat transfer.

Author Contributions: Conceptualization, Y.Z. and Z.W.; methodology, Y.Z. and Z.W.; formal analysis, W.Q., P.Z., R.B., and X.M.; investigation, P.Z. and W.Q.; writing—original draft preparation, Y.Z. and Z.W.; writing—review and editing, Z.W.; visualization, W.Q. and X.Z.; supervision, Y.Z. and Z.W.; project administration, Y.Z., Z.W., and X.Z.; funding acquisition, Z.W. All authors have read and agreed to the published version of the manuscript.

Funding: This research was funded by the Natural Science Foundation of Hunan Province, grant numbers 2022JJ40618 and 2023JJ60619.

Data Availability Statement: The data presented in this study are available in the article.

Conflicts of Interest: The authors declare no conflicts of interest.

Appendix A

Table A1. List of parameters used for the calculation and their values.

	Parameter	Value (Fir)	Value (Oak)
T_p	Pyrolysis temperature	588 K [28]	600 K [37]
k_g	Thermal conductivity of air ($T = (T_f + T_p)/2$)	0.064 W/(m·K) [41]	0.0549 W/(m·K) [41]
T_{char}	Characteristic temperature	920.5 K	926.5 K
t_{ig}	Ignition time (natural wood)	26.5 s [28]	57 s [45]
c_p	Heat capacity of wood	1.380 kJ/(kg·K) [28]	1.255 kJ/(kg·K) [35]
ΔH_c	Heat of combustion of pyrolyzed gases	12.0 MJ/kg [46]	15.2 MJ/kg
α	Thermal diffusivity ($T = (T_f + T_p)/2$)	1.55×10^{-4} m^2/s [41]	1.09×10^{-4} m^2/s [41]
ν	Kinematic viscosity ($T = (T_f + T_p)/2$)	1.122×10^{-4} m^2/s [41]	0.7637×10^{-4} m^2/s [41]
ρ_∞	Density of air ($T = (T_f + T_p)/2$)	0.367 kg/m^3 [41]	0.4643 kg/m^3 [41]
ρ_0	Density of natural wood	446.67 kg/m^3	731.20 kg/m^3
$c_{p,\infty}$	Heat capacity of air ($T = (T_f + T_p)/2$)	1.131 kJ/(kg·K) [41]	1.087 kJ/(kg·K) [41]
h	Heat transfer coefficient ($T = (T_f + T_p)/2$)	3.69 W/(m^2·K)	3.61 W/(m^2·K)
k_y	Radial thermal conductivity (natural wood)	0.1589 W/(m·K)	0.1625 W/(m·K)
z	The ratio of volume to surface area	9.58×10^{-4} m	
g	Gravity acceleration	9.8 m/s^2	
σ	Stefan–Boltzmann constant	5.678×10^{-8} W/(m^2·K^4)	
T_f	Flame temperature	1253 K	
T_∞	Ambient temperature	300 K	
T_s	Initial wood surface temperature	300 K	
β	Thermal expansion coefficient	1.18×10^{-3} K^{-1} [41]	
θ	Flame tilt angle	90°	
W	Width of wood	0.05 m	
d	Thickness of wood	0.002 m	

References

1. Chen, C.; Kuang, Y.; Zhu, S.; Burgert, I.; Keplinger, T.; Gong, A.; Li, T.; Berglund, L.; Eichhorn, S.J.; Hu, L. Structure–Property–Function Relationships of Natural and Engineered Wood. *Nat. Rev. Mater.* **2020**, *5*, 642–666. [CrossRef]
2. Bäcklund, K.; Molinari, M.; Lundqvist, P. In Search for Untapped Energy-Saving Potential in Green and Smart Higher Educational Buildings—An Empirical Case Study Involving the Building Occupants. *Buildings* **2023**, *13*, 3103. [CrossRef]
3. Li, T.; Zhai, Y.; He, S.; Gan, W.; Wei, Z.; Heidarinejad, M.; Dalgo, D.; Mi, R.; Zhao, X.; Song, J.; et al. A Radiative Cooling Structural Material. *Science* **2019**, *364*, 760–763. [CrossRef]
4. Fan, C.; Gao, Y.; Li, Y.; Yan, L.; Zhuang, Y.; Zhang, Y.; Wang, Z. A Flame-retardant and Optically Transparent Wood Composite. *J. Appl. Polym. Sci.* **2022**, *139*, e52945. [CrossRef]
5. Tollefson, J. The Wooden Skyscrapers That Could Help to Cool the Planet. *Nature* **2017**, *545*, 280–282. [CrossRef]
6. Namari, S.; Drosky, L.; Pudlitz, B.; Haller, P.; Sotayo, A.; Bradley, D.; Mehra, S.; O' Ceallaigh, C.; Harte, A.M.; El-Houjeyri, I.; et al. Mechanical Properties of Compressed Wood. *Constr. Build. Mater.* **2021**, *301*, 124269. [CrossRef]
7. Gan, W.; Chen, C.; Wang, Z.; Song, J.; Kuang, Y.; He, S.; Mi, R.; Sunderland, P.B.; Hu, L. Dense, Self-Formed Char Layer Enables a Fire-Retardant Wood Structural Material. *Adv. Funct. Mater.* **2019**, *29*, 1807444. [CrossRef]
8. Yuan, S.; Xiang, K.; Yan, F.; Liu, Q.; Sun, X.; Li, Y.; Du, P. Characteristics and Mechanism of Fire Spread between Full-Scale Wooden Houses from Internal Fires. *Buildings* **2022**, *12*, 575. [CrossRef]
9. Wang, H.; Gong, J.; Wang, H.; Gong, J. A Comparative Study of GA, PSO and SCE Algorithms for Estimating Kinetics of Biomass Pyrolysis. *Emerg. Sci. Technol.* **2023**, *3*, 9. [CrossRef]
10. Kollmann, F.; Cote, W. Solid Wood. In *Principles of Wood Science and Technology*; Springer: Berlin/Heidelberg, Germany; New York, NY, USA, 1968.
11. Zhou, Y.; Zhou, P.; Bu, R.; Zhang, X.; Chu, T.; Wang, Z. Horizontal Flame Spread Behavior of Densified Wood: Effect of Structural Characteristics. *Fuel* **2024**, *362*, 130687. [CrossRef]
12. Wang, H.; Wang, Z.; Wen, L.; Meng, H.; Wang, W.; Huang, X. The Flame Spread Performance over Discrete Wooden Chips Varying Wood Species. *Therm. Sci. Eng. Prog.* **2023**, *39*, 101674. [CrossRef]

13. Jiang, L.; He, J.-J.; Sun, J.-H. Sample Width and Thickness Effects on Upward Flame Spread over PMMA Surface. *J. Hazard. Mater.* **2018**, *342*, 114–120. [CrossRef]
14. Zhao, L.; Fang, J.; He, X.; Wang, J.; Tao, S.; Zhang, Y. An Analysis of Width Effects on Flame Spread in Conjunction with Concurrent Forced Flow Using a Variable B-Number. *Combust. Flame.* **2018**, *194*, 334–342. [CrossRef]
15. Wang, Q.; Xiao, H.; Wan, W.; Cui, Z.; Zhu, H.; Sun, J. Flame Spread on Inclined Wood Surfaces: Influence of External Heat Flux and Ambient Oxygen Concentration. *Combust. Sci. Technol.* **2018**, *190*, 97–113. [CrossRef]
16. Zhou, J.; Zhu, G.; Gao, Y.; Gao, S.; Chai, G. Experimental Study on the Effects of Width and Self-Extinguishing on the Upward Flame Spread for Linen Fabric. *Case Stud. Therm. Eng.* **2019**, *14*, 100500. [CrossRef]
17. Saito, K.; Williams, F.A.; Wichman, I.S.; Quintiere, J.G. Upward Turbulent Flame Spread on Wood Under External Radiation. *J. Heat Transf.* **1989**, *111*, 438–445. [CrossRef]
18. Fernandez-Pello, A.C.; Ray, S.R.; Glassman, I. Flame Spread in an Opposed Forced Flow: The Effect of Ambient Oxygen Concentration. *Symp. Int. Combust.* **1981**, *18*, 579–589. [CrossRef]
19. Song, J.; Chen, C.; Zhu, S.; Zhu, M.; Dai, J.; Ray, U.; Li, Y.; Kuang, Y.; Li, Y.; Quispe, N.; et al. Processing Bulk Natural Wood into a High-Performance Structural Material. *Nature* **2018**, *554*, 224–228. [CrossRef]
20. Richter, F.; Rein, G. A Multiscale Model of Wood Pyrolysis in Fire to Study the Roles of Chemistry and Heat Transfer at the Mesoscale. *Combust. Flame.* **2020**, *216*, 316–325. [CrossRef]
21. Yi, L.; Zhuang, Y.; Ding, Y.; Gong, J.; Chu, T.; Wang, Z. Influence of Component Fractions and Structure Characteristic on the Combustion Behavior of Densified Wood. *Fire Saf. J.* **2024**, *144*, 104086. [CrossRef]
22. Blasi, C.D.; Wichman, I.S. Effects of Solid-Phase Properties on Flames Spreading over Composite Materials. *Combust. Flame* **1995**, *102*, 229–240. [CrossRef]
23. Kobayashi, Y.; Terashima, K.; Oiwa, R.; Tokoro, M.; Takahashi, S. Opposed-Flow Flame Spread over Carbon Fiber Reinforced Plastic under Variable Flow Velocity and Oxygen Concentration: The Effect of in-Plane Thermal Isotropy and Anisotropy. *Proc. Combust. Inst.* **2021**, *38*, 4857–4866. [CrossRef]
24. Quintiere, J. A Simplified Theory for Generalizing Results from a Radiant Panel Rate of Flame Spread Apparatus. *Fire Mater.* **1981**, *5*, 52–60. [CrossRef]
25. Amaral, S.S.; de Carvalho, J.A., Jr.; Costa, M.A.M.; Neto, T.G.S.; Dellani, R.; Leite, L.H.S. Comparative Study for Hardwood and Softwood Forest Biomass: Chemical Characterization, Combustion Phases and Gas and Particulate Matter Emissions. *Bioresour. Technol.* **2014**, *164*, 55–63. [CrossRef] [PubMed]
26. Hao, H.; Chow, C.L.; Lau, D. Effect of Heat Flux on Combustion of Different Wood Species. *Fuel* **2020**, *278*, 118325. [CrossRef]
27. Chen, Y.; Hao, Y.; Wang, J.; Gao, H.; Liu, G.; Lan, B.; Zhang, Y.; Chen, J. Effect of Ambient Temperature and Wind Speed on Horizontal Flame Spread and Combustion Trace on Typical Decorative Wood Boards. *Constr. Build. Mater.* **2023**, *408*, 133597. [CrossRef]
28. Wang, Z.; Gao, Y.; Zhou, Y.; Fan, C.; Zhou, P.; Gong, J. Pyrolysis and Combustion Behaviors of Densified Wood. *Proc. Combust. Inst.* **2023**, *39*, 4175–4184. [CrossRef]
29. Fan, C.; Gao, Y.; Li, Y.; Yan, L.; Zhu, D.; Guo, S.; Ou, C.; Wang, Z. A Flame-Retardant Densified Wood as Robust and Fire-Safe Structural Material. *Wood Sci. Technol.* **2023**, *57*, 111–134. [CrossRef]
30. Yan, W.G.; Wang, C.J.; Guo, J. One Extended OTSU Flame Image Recognition Method Using RGBL and Stripe Segmentation. *Appl. Mech. Mater.* **2011**, *121–126*, 2141–2145. [CrossRef]
31. Otsu, N. A Threshold Selection Method from Gray-Level Histograms. *IEEE Trans. Syst. Man Cybern.* **1979**, *9*, 62–66. [CrossRef]
32. Zukoski, E.E.; Cetegen, B.M.; Kubota, T. Visible Structure of Buoyant Diffusion Flames. *Symp. Int. Combust.* **1985**, *20*, 361–366. [CrossRef]
33. Hasemi, Y. Experimental Wall Flame Heat Transfer Correlations for the Analysis of Upward Wall Flame Spread. *Fire Sci. Technol.* **1984**, *4*, 75–90. [CrossRef]
34. Gao, Z.H.; Liu, Z.X.; Ji, J.; Fan, C.G.; Li, L.J.; Sun, J.H. Experimental Study of Tunnel Sidewall Effect on Flame Characteristics and Air Entrainment Factor of Methanol Pool Fires. *Appl Therm. Eng.* **2016**, *102*, 1314–1319. [CrossRef]
35. Flity, H.; Jannot, Y.; Terrei, L.; Lardet, P.; Schick, V.; Acem, Z.; Parent, G. Thermal Conductivity Parallel and Perpendicular to Fibers Direction and Heat Capacity Measurements of Eight Wood Species up to 160 °C. *Int. J. Therm. Sci.* **2024**, *195*, 108661. [CrossRef]
36. *ISO 13061-1*; Physical and Mechanical Properties of Wood—Test Methods for Small Clear Wood Specimens, Part 1: Determination of Moisture Content for Physical and Mechanical Tests. International Organization for Standardization: Geneva, Switzerland, 2017.
37. Figueiredo, J.L.; Valenzuela, C.; Bernalte, A.; Encinar, J.M. Pyrolysis of Holm-Oak Wood: Influence of Temperature and Particle Size. *Fuel* **1989**, *68*, 1012–1016. [CrossRef]
38. Leventon, I.T.; Stoliarov, S.I. Evolution of Flame to Surface Heat Flux during Upward Flame Spread on Poly(Methyl Methacrylate). *Proc. Combust. Inst.* **2013**, *34*, 2523–2530. [CrossRef]
39. Beaulieu, P.A.; Dembsey, N.A. Effect of Oxygen on Flame Heat Flux in Horizontal and Vertical Orientations. *Fire Saf. J.* **2008**, *43*, 410–428. [CrossRef]
40. Zhang, Y.; Ji, J.; Li, J.; Sun, J.; Wang, Q.; Huang, X. Effects of Altitude and Sample Width on the Characteristics of Horizontal Flame Spread over Wood Sheets. *Fire Saf. J.* **2012**, *51*, 120–125. [CrossRef]

41. Incropera, F.P.; DeWitt, D.P.; Bergman, T.L.; Lavine, A.S. *Fundamentals of Heat and Mass Transfer*; Wiley: New York, NY, USA, 2007.
42. Cai, M.; Chen, S.; Tang, Y.; Li, Q.; An, W. Study on the Influence of Enclosed Vertical Channels on Downward Flame Spread over XPS Thermal Insulation Materials. *Case Stud. Therm. Eng.* **2019**, *14*, 100486. [CrossRef]
43. Quintiere, J.G. *Fundamentals of Fire Phenomena*; John Wiley & Sons: Hoboken, NJ, USA, 2006.
44. Rossi, J.-L.; Chetehouna, K.; Collin, A.; Moretti, B.; Balbi, J.-H. Simplified Flame Models and Prediction of the Thermal Radiation Emitted by a Flame Front in an Outdoor Fire. *Combust. Sci. Technol.* **2010**, *182*, 1457–1477. [CrossRef]
45. Shi, L.; Chew, M.Y.L. Experimental Study of Woods under External Heat Flux by Autoignition: Ignition Time and Mass Loss Rate. *J. Therm. Anal. Calorim.* **2013**, *111*, 1399–1407. [CrossRef]
46. Hostikka, S.; Matala, A. Pyrolysis Model for Predicting the Heat Release Rate of Birch Wood. *Combust. Sci. Technol.* **2017**, *189*, 1373–1393. [CrossRef]